Asian Journal of Chemistry; Vol. 37, No. 9 (2025), 2313-2321
ASIAN JOURNAL OF CHEMISTRY
https://doi.org/10.14233/ajchem.2025.34377

Anticorrosivity of Electroless Ni-P-TiO_2 Nanoplatings against Hydrogen Peroxide Solution

ARVIND KUMAR[1,*], ABHISHEK GUPTA[2], PRASHANT SINGH[3], SULAXNA SHARMA[4] and AWANISH SHARMA[1]

[1]Department of Physics, Graphic Era Deemed to be University, Dehradun-248001, India
[2]Department of Chemistry, D.B.S. (PG) College, Dehradun-248001, India
[3]Department of Chemistry, D.A.V. (PG) College, Dehradun-248001, India
[4]Department of Applied Science & Humanities, THDC Institute of Hydropower Engineering and Technology, Bhagirathi Puram, Tehri-249001, India

*Corresponding author: E-mail: arvindkumardbsphy@gmail.com

Received: 1 July 2025 *Accepted*: 16 August 2025 *Published online*: 30 August 2025 AJC-22114

The pollution regulator measurements have resulted replacement of chlorine/chlorine dioxide through hydrogen peroxides as bleaching chemicals specially in paper, dye and textile industries. Adaptation of changed chemicals, generally affects the corrosion aspects, suitability of existing plant metallurgy, materials of construction of equipment and environmental conditions. The surface platings besides non-sactrificial, recently have acted as an obstacle between steel substrates and corrosive environments. Accordingly, a long-term immersion and electrochemical corrosion tests were conducted on steels (MS, SS 316L) and electroless plated Ni-P and Ni-P-TiO_2 nanomaterials in hydrogen peroxide solutions at pH 9.1 ± 0.1 and an E-pH was diagram drawn for H_2O-H_2O_2 system alongside Shannon entropy values were calculated by MATLAB software and are used to understand the corrosivity of the peroxide media and protection mechanism of tested materials. On the basis of long-term immersion corrosion test, electrochemical corrosion tests, an H_2O-H_2O_2 E-pH diagram, Shannon entropy values and cost to mechanical properties; the different tested materials may be graded in terms of their resistance against uniform/localized type corrosion for handling peroxide test media in following manner: Ni-P-TiO_2 as-plated > Ni-P-TiO_2 heated > Ni-P as-plated > Ni-P heated ~SS316L > MS. The better cost/strength ratio of Ni-P-TiO_2 platings make these materials as more suitable for handling peroxide media with/without Cl content.

Keywords: Steels, Electroless nickel, E-pH, Hydrogen peroxide, Shannon entropy, Corrosion.

INTRODUCTION

The steel materials are well known for their good strength and corrosion resistance however these materials have been found rapidly deteriorated in those environments which contains chemicals like sulphides, peroxides, nitrates, chlorides, high temperature and pressure as well as acidic/alkaline pH, *etc*. [1]. The surface platings can act as a barrier between steels substrates and corrosive environments and are also frequently non-sactrificial [2]. Earlier in 1946, the electroless nickel (EN) based surface platings were developed by Brenner & Riddell and thought out a very promising approach to protect steel materials. These platings were also used extensively into several industries such as petrochemical, electronics, automobile, paper, marine, space, nuclear and other engineering applications owing to their desirable characteristics such as tremendous hardness, high adhesion, homogenous plating, weldability, low cost, promising wear and corrosion resistance, *etc*. [3,4]. Fundamentally, the EN platings combines the catalytic reduction of metallic ions into a reducing agent containing an aqueous solution and subsequently the metal's deposition occurs in absence of any outside energy source [5].

Later on, more eco-friendly electroless nickel-phosphorus (EL Ni-P) surface platings were developed for enriching the mechanical and electrochemical characteristics of EN platings [6]. In electroless EL Ni-P deposition mechanism, the three key chemical reactions such as occurs inside electroless bath and finally the Ni-P is deposited on a fine sensitized ($SnCl_2$) and activated ($PdCl_2$) substrate surface [7].

$$H_2PO_2^- + H_2O \rightarrow HPO_3^{2-} + H^+ + 2H_{ads} \quad (1)$$

$$2H_{ads} + Ni^{2+} \rightarrow Ni + 2H^+ \quad (2)$$

$$H_2PO_2^- + H_{ads} \rightarrow H_2O + OH^- + P \quad (3)$$

Well ahead with more fabulous advancements into the nanoscience and nanotechnology, addition of certain soft and hard solid inorganic nanoparticles *e.g*. polytetrafluoroethylene (PTFE), titanium nitride (TiN), ZnO, Al_2O_3, ZrO_2, C_3N_4, MoS_2, TiO_2, SiO_2, SiC, W, ZnO, boron nitride (BN), Si_3N_4, TiNi (nitinol), tungsten carbide (WC), carbon nanofiber (CNF), *etc*. into the EL Ni-P platings have further enhanced their electrochemical, mechanical, electronics, optical, antibacterial, *etc*. characteristics [8-15]. Moreover, the shape, size, concentration of these reinforced inorganic soft and hard nanoparticles particles, heat treatment processes, *etc*. have significantly affected the microstructures of novel electroless Ni-P composite platings as well as their electrochemical, mechanical, optical and antibacterial properties [16]. Among above mentioned several inorganic soft and hard nanoparticles, the TiO_2 nanoparticles have fascinated the scientists for their remarkable anticorrosion, tribological, photocatalytic mechanism and antimicrobial applications [17-20]. Chemically, the TiO_2 material has three phases (anatase, rutile both tetragonal structure; and brookite, orthorhombic structure) and is considered a much-valued semiconducting transition metal oxide with its molecular weight 79.866 g/mol, melting point 2116 K, energy band gap 3.15 to 3.21 eV, and mass density 3.78 to 4.23 g/cm^3. Moreover, the TiO_2 nanoparticles displays some other exceptional features, such as easy mechanism, large surface area to volume ratio, excellent surface morphology, reduced cost, non-toxic and good resistance to chemical erosion, *etc*. [21].

In one study, the mechanism of pathogenic inactivation through TiO_2 nanoparticles has been correlated with light absorption, hole-electron pair generation and oxidation of organic substances through superoxide anions (O_2^-)/hydroxyl (OH^-) radicals, *etc*. [22]. The electroless Ni-P and Ni-P-TiO_2 platings were deposited on carbon-steel substrates and found that TiO_2 modified film have significant improved tribological characteristics and corrosion resistance into H_2SO_4 and NaCl solutions as compared to elecroless Ni-P platings [23]. Hasan *et al*. [24] found enhanced microhardness (1025 HV200) as well as wear resistance into novel Ni-P-TiO_2 plating deposited on AZ31 Mg alloy than the conventional Ni-P-TiO_2 (710 HV200) composite plating. In another study, the electroless Ni-P-TiO_2 plating deposited on API-5L-X65 steel substrate has found to be enhanced microhardness but lower corrosion resistance than Ni-P plating [25]. Further, the TiO_2/TeO_2 nanopowders were attained through an aqueous sol-gel technique and these nanopowders exhibited good antimicrobial activity against *E. coli* K12 bacteria [26]. Furthermore, another type of the nanoplatings like Ni-B-TiO_2 have shown improved tribological and microhardness as compared to Ni-B plating [27]. John *et al*. [28] compared the corrosion resistance of three types of electroless platings such as Ni-P, Ni-P-TiO_2 and NiP-TiO_2-NiP platings into 3.5% NaCl solution to analyze and found that the multi-layer NiP-TiO_2-NiP plating has enhanced significant corro-sion resistance than other platings.

The TiO_2 nanomaterials prepared by chemical vapor deposition (CVD), physical vapor deposition (PVD) and electrodeposited methods have also demonstrated vast possibility into enhancement of optical, chemical, antibacterial, tribological, anticorrosion and antifungal properties [5,9,16-22]. The electroless plating method has easy plating mechanism, can plate the intricate part of a geometry, low cost, non-toxic and less space requirement and while on the other side, the titanium dioxide (TiO_2) nanoparticles are known for their anticorrosion, tribological as well as antimicrobial applications. In this research, Ni-P and Ni-P-TiO_2 nanocomposite coatings were deposited on low-cost mild steel (AISI 1040) substrates using an electroless plating method. The structural morphology, composition and phase changes during the heat treatment process were analyzed using FESEM and XRD techniques. Moreover, the corrosion resistance behavior of Ni-P/Ni-P-TiO_2 composite platings and conventional steel materials into peroxide solutions (pulp bleached chemical into paper industry) have been examined by a long duration (six month) weight loss corrosion test and electrochemical corrosion tests. In addition, an E-pH diagram for H_2O-H_2O_2 system has been constructed to understand the corrosion protection mechanism of developed materials in the peroxide corrosion test solutions. Moreover, as the texture aspect ratio assesses isotropicity and grain growth mechanisms during sintering process of nanocomposite surfaces and differences in these images can be categorized by using entropy, which is more sensitive to magnification levels or pixel numbers [29]. The Shannon entropy quantifies system dimensions effectively using a logarithm for additive representation and comparing images of various magnifications is viable with a normalized figure of merit. The Shannon entropy is represented by H(α) or H, and it quantifies uncertainty in a random variable α, and p_i (α) is probability of an event:

$$H(\alpha) = -\Sigma[p_i(\alpha) * \log_2(p_i)] \quad (4)$$

This formula shows the multiplicative probabilities converted to additive entropy [30,31]. Therefore, the surface morphology of both as-plated and heated Ni-P-TiO_2 platings were analyzed by MATLAB software/program using FESEM images through Shannon entropy values and their results are also correlated with corrosion resistance.

EXPERIMENTAL

For electroless Ni-P/Ni-P-TiO_2 depositions on mild steel (MS; AISI 1040) substrate surface, the mild steel coupons dimensions were selected as 20 mm length, 20 mm width, 3 mm to 4 mm thickness and initially were dipped into 50% HCl solution for 30 sec to get rid of any surface rust. After it, these mild steel (MS) coupons were washed with distilled water and later on mirror polished by SiC emery paper of 60 to 1200 grit as well as degreased by acetone solution before plating [32]. For electroless deposition process, the well-polished cleaned mild steel (MS) coupons were first sensitized by 1% aqueous $SnCl_2$ solution for 120 sec and subsequently activated through a mild hot $PdCl_2$ solution (55 ºC) for 30 sec and further followed by distilled water washing and air dry. Now the well activated MS coupon for Ni-P/Ni-P-TiO_2 deposition is dipped into electroless bath solution whose composition, concentration and operating parameters are presented in Tables 1 and 2 [33]. The plating thickness (t) was calculated from eqn. 5:

$$\text{Coating thickness } (\mu m) = \frac{\text{Weight increase (g)} \times 10^4}{\text{Density (7.75 g/cm}^3) \times \text{Surface area of deposition (cm}^2)} \quad (5)$$

TABLE-1
CHEMICALS CONCENTRATIONS AND OTHER OPERATING PARAMETERS FOR ELECTROLESS BATH

Chemicals nomenclature	Obstinacy of chemicals	Amounts (for 100 mL deionized-water)
$NiSO_4.6H_2O$ (Nickel-sulphate, Sigma-Aldrich grade)	Ni^{2+} cations source	03.31 ± 0.02 g
$C_6H_5Na_3O_7 \cdot 2H_2O$ (Tri-sodium- citrate, Merck grade)	Controlled discharge of Ni^{2+} cations	06.41 ± 0.02 g
NH_3 solution Buffered by (NH_4SO_4, Sd-fine + NH_4Cl, Merck-grade)	Maintain pH 8.2 ± 0.1	03.10 ± 0.02 g each
NaOH/CH_3COOH, 5% solution	Maintain pH, while chemical reaction on	Drop-wise addition
$NaH_2PO_2 \cdot H_2O$ (Sodium- hypophosphite, Loba-grade)	Act as reducer to Ni^{2+} cations	02.53 ± 0.02 g
TiO_2 (Titania) nanoparticles (Merck, size range 50 to 80 nm, density 4.03 g/cm^3, surface area16500 ± 15.8 nm^2)	A reinforcement into Ni-P matrix for antibacterial application	00.25 ± 0.01 g
Bath operating environments, surfactant as sodium dodecyl sulfate ($NaC_{12}H_{25}SO_4$) = 0.1 g/L	–	80 ± 2 ºC, constant stirring, 270 rpm
Annealing process	To understand significances of heating	380 ± 2 ºC under Argon environment for one- hour duration

TABLE-2
COMPOSITION OF STEEL MATERIALS FOR WEIGHT LOSS AND ELECTROCHEMICAL CORROSION TESTS

Alloys	C	Cr	Ni	Mo	P	Cu	Mn	S	Si	N
MS	0.18	–	–	–	–	–	1.66	–	0.04	–
SS316L	0.019	17.43	11.26	2.03	0.027	0.40	1.11	0.002	0.50	0.048

*Fe balance

After completion of deposition, the plating thickness values were found in the range of 8.3 to 17.8 µm [16-18,25]. The microstructure and constituent composition of as-plated and heated (380 ºC) Ni-P/Ni-P-TiO_2 specimens were also evaluated by the help of FESEM/EDAX techniques (ZEISS EVO18-FESEM instrument) [17-20,23-26]. Their X-ray diffraction study (XRD, Bruker AXS D8 advance powder diffractometer, accelerating voltage 40 kV, charge per unit time 30 mA, Cu-*K*α radiation having wavelength λ = 1.541Å) was carried out [21,22]. The grains dimensions of the electroless deposited specimens were calculated by using a Scherrer equation (t = 0.9λ/Bcos θ) where parameter λ is Cu*K*α wavelength (λ = 1.54 Å), B is broadening of full width at half maximum furthermore, θ is the Bragg's angle by intense Ni (111) peak (after removal of instrumental broadening cause [23,24,3-36].

For long term weight loss and electrochemical corrosion tests at room temperature, all steels (MS, SS316L) and Ni-P/Ni-P-TiO_2 plated coupons are exposed into an alkaline (pH 9.1 ± 0.1) peroxide (H_2O_2) media with subjective chloride and peroxide concentration. The composition of corrosion test solutions was further analyzed for peroxide and chloride concentration using reported methods [37]. In long term corrosion immersion test besides corrosion rate and pit depth measureement, each coupon was also fitted by Teflon serrated washers for commencing crevice corrosion attack. During the immersion corrosion test, pH, H_2O_2 and Cl contents of test solutions were examined and keep up daily. Throughout the corrosion test phase, the quantity of H_2O_2 has been found decreased in variation of 4.1 ± 2.3%, Cl^- decreased in variation of 3.8 ± 2.1% and that of pH increased from 1.6 ± 0.2% from their individual initial mark values as depicted into Table-3. After the long exposure of test coupons into peroxide solutions, the corroded specimens were first cleaned mechanically and later on dipped into cold solution of conc. HCl plus 20 g/L $SbCl_3$ and 50 g/L $SnCl_2$ [32,38]. The cleaned corroded specimens were then weighed for estimating weight loss so as to establish the corrosion rate by means of an equation as:

$$\text{Corrosion rate (mpy)} = \frac{3.45\times10^6 \times \text{Weight loss (g)}}{\text{Density of metal (g/cm}^3)\times \text{Exposure time (h)}\times \text{Area (cm}^2)} \quad (6)$$

Further, for the measurement of corrosion potential (E_{corr}), pitting potential, passivation range (MOS) and also to understand surface layer protection mechanism, the electrochemical corrosion tests namely open circuit potential (OCP), potentiodynamic, cyclic polarization tests were recorded in peroxide solutions at room temperature and an E-pH diagram was also constructed. In electrochemical measurements, the anodic polarization curves were traced with a scanning rate of 0.16 mV/s from -500 mV to +1800 mV with respect to saturated calomel electrode (SCE; reference electrode), graphite rod (auxiliary electrode) and test specimen (working electrode). The all corroded specimens were also examined by an optical metallurgical microscope (make: Riechert Jung, USA) for evaluating pitting depth and crevice type corrosion attack by measuring the utmost depth of attack [2,16,24,32,36-41].

TABLE-3
COMPOSITION AND CONCENTRATION FOR CORROSION TEST SOLUTIONS (pH 9.1 ± 0.1)

Chemicals	Solution 1	Solution 2	Solution 3	Solution 4
Peroxide (ppm)	370 ± 0.8	370 ± 0.8	740 ± 0.8	740 ± 0.8
Chloride (ppm)	0	1000 ± 0.6	0	1000 ± 0.6

RESULTS AND DISCUSSION

Characterization of platings: In physical appearance after removing the plated Ni-P/Ni-P-TiO_2 coupons from the electroless deposition bath, the Ni-P platings revealed a white glossy silvery appearance whereas the as-plated Ni-P-TiO_2 nanocomposite have shown a slightly blurred silvery presence. The SEM micrograph of as-plated Ni-P coupon illustrates a cauliflower like structure in addition consisting of fine nodules and while in as-plated Ni-P-TiO_2 coupon, the TiO_2 nanoparticles as white spherical globules are found generally uniformly dispersed however with some agglomeration at some places into electroless Ni-P matrix (Fig. 1). This phenomenon points out toward amorphous structure for as-plated Ni-P/Ni-P-TiO_2 platings. Further after heat treatment of as-plated Ni-P/Ni-P-TiO_2 coupon at 380 ºC for 1 h under argon atmosphere, the spherical nodules into heated Ni-P/ Ni-P-TiO_2 plating turn out to be more and larger indicating a more deposition of nickel and TiO_2 nanoparticles into electroless Ni-P matrix and characterizes semi-crystalline structure for these heated platings [17-23]. The findings of the EDAX study in Ni-P platings aroused not much difference between plating elements, though if compared as-coated Ni-P-TiO_2 coupons with heated Ni-P-TiO_2 coupons, the amounts of iron (Fe, 02.41 ± 0.13) has been found slightly increased, and while the quantity of other plating constituents (Ni: 79.28 ± 0.06, O: 04.63 ± 0.07, P: 11.04 ± 0.08, and Ti: 02.06 ± 0.09, C: 0.28 ± 0.03) has been reduced in all heated Ni-P-TiO_2 coupons (Fig. 2). These outcomes for heated Ni-P-TiO_2 coupons could be because of different intermetallics (Ni-P, Ni-Ti, *etc.*) formation and internal dispersal of plating element Ni and Ti during heating process, which can be seen as less number of white globules in heated platings. Moreover, the presence of iron (Fe) and carbon (C) in these platings could be found due to MS coupon composition (Table-4) [4,7,17-26]. The XRD spectra of as-plated and heated Ni-P-TiO_2 deposits have illustrated main diffracted Ni_3P corresponding to at 2θ angle 43.9º for as-coated 44.2º for heated deposits (JCPDS card no. 01-074-1384). The TiO_2 anatase (A) phase for as-plated Ni-P-TiO_2 coatings is observed mainly for plane (101) at 2θ angle 26.2º, (004) plane at 37.3º and (200) plane at 48.3º while for heated Ni-P-TiO_2 deposits for plane (101) at 2θ angle 26.3º, (004) plane at 37.5º and (200) plane at 48.5º (JCPDS card no. 21-1272). The physical morphological alterations from amorphous phase to crystalline phase can origin some sharpening of peaks and slight shift of angles towards higher side into heated Ni-P-TiO_2 deposits (Fig. 3). The breadth of main peak

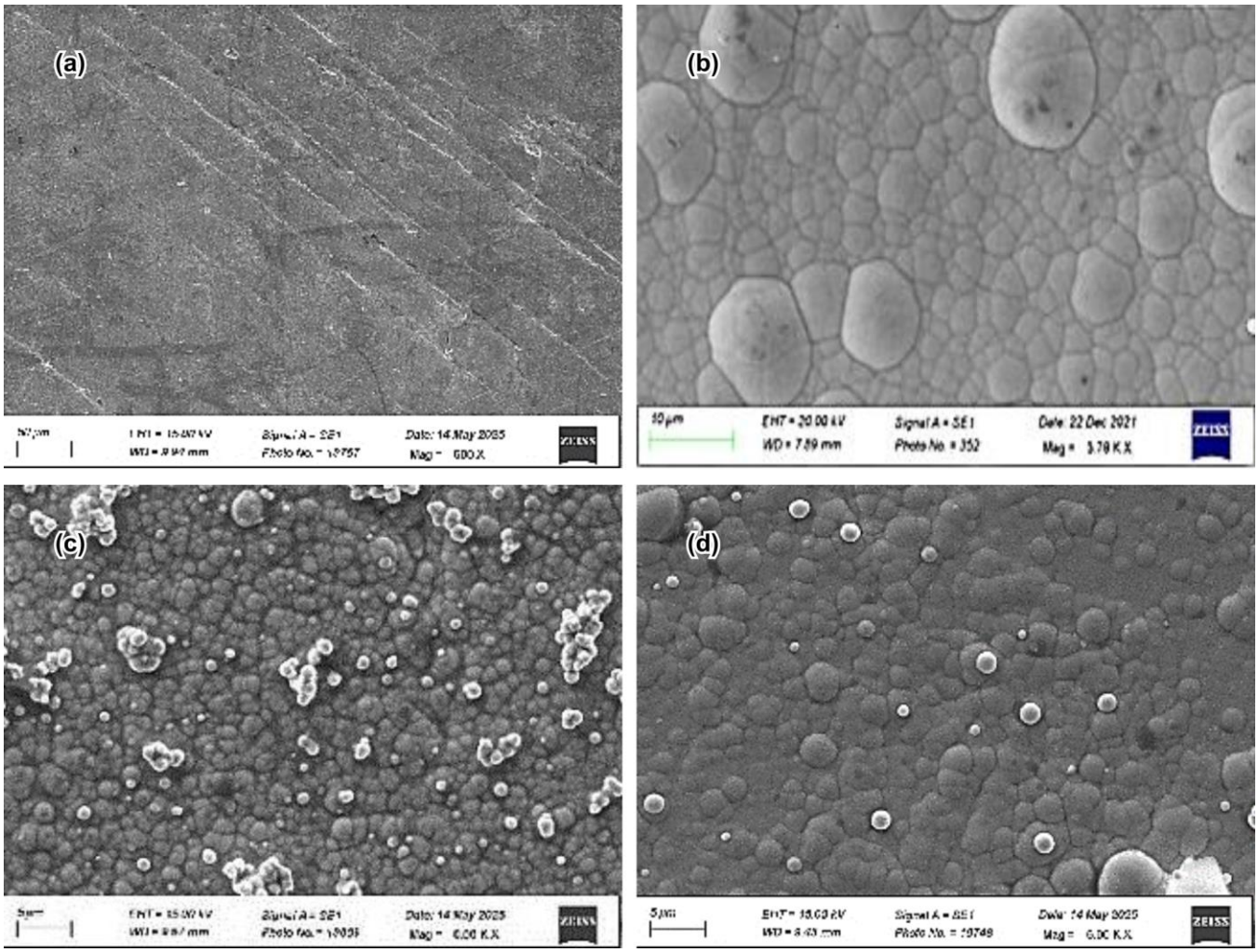

Fig. 1. SEM micrographs of (a) MS (b) Ni-P heated (c) Ni-P-TiO_2 as-plated and (d) Ni-P-TiO_2 heated platings

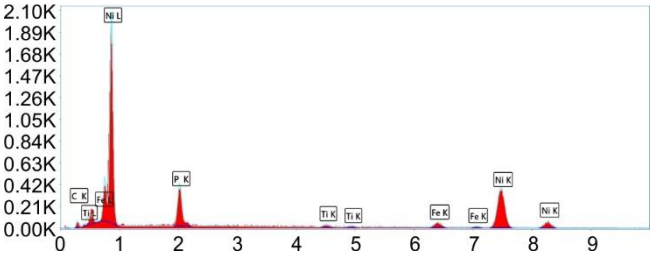

Fig. 2. EDAX micrograph for Ni-P-TiO_2 nanocomposite plating (heated)

of Ni (111) point out grain proportions are in range of 5 to 14 nm [3,8,17-26,34,35].

Corrosion studies: For corrosion investigations, initially a Pourbaix (Potential-pH) diagram was constructed for H_2O-H_2O_2 system considering only those electrochemical reactions, which can be mainly accountable for corrosion of tested materials in present peroxide test solutions, the graphene-based gel retains around 70% water content. This observed shrinkage is likely due to the decreased interlayer spacing associated with the reduction of GO to graphene.

$$H_2O_2 \leftrightarrow HO_2^- + H^+ \quad (7)$$

Equivalent Nernst equation:

$$\log\left(\frac{HO_2^-}{H_2O_2}\right) = pH - 11.63$$

$$2H_2O \leftrightarrow H_2O_2 + 2H^+ + 2e^- \quad (8)$$

Equivalent Nernst equation:

$$E_{HO_2^-/H_2O} = 1.78 - 0.059\ pH + 0.0295 \log\ [H_2O_2]$$

$$2H_2O \leftrightarrow HO_2^- + 3H^+ + 2e^- \quad (9)$$

Equivalent Nernst equation:

$$E_{HO_2^-/H_2O} = 2.12 - 0.089\ pH + 0.0295 \log\ [HO_2^-]$$

$$H_2O_2 \leftrightarrow O_2 + 2H^+ + 2e^- \quad (10)$$

Equivalent Nernst equation:

$$E_{O_2/H_2O_2} = 0.68 - 0.059\ pH + 0.0295 \log\ [P_{O_2}/H_2O_2]$$

$$HO_2^- \leftrightarrow O_2 + H^+ + 2e^- \quad (11)$$

Equivalent Nernst equation:

$$E_{O_2/HO_2^-} = 0.34 - 0.0295\ pH + 0.0295 \log\ [P_{O_2}/HO_2^-]$$

In the E-pH diagram, the amount of H_2O_2 was taken as 370 ppm and 740 ppm and a vertical thick line at pH 9.1 is mainly indicating the range of open circuit potential (OCP) values for different steels and Ni-P/Ni-P-TiO_2 plated coupons (Fig. 4). As the OCP's range measured electrochemically for all tested materials into peroxide solutions is lying near line 4 (370 ppm) and line 4′ (740 ppm), therefore H_2O_2/O_2 equilibrium will be responsible for following reduction reactions:

$$H_2O_2 + 2H^+ + 2e^- \rightarrow 2H_2O \quad (12)$$

$$O_2 + 4H^+ + 4e^- \rightarrow 2H_2O \quad (13)$$

Due to higher reduction potential of H_2O_2, it will dominate more in comparison to O_2 in influencing the corrosion of steels and Ni-P/Ni-P-TiO_2 plated materials and which consequently might result an increase into pH of peroxide test solutions. This slight upsurge into pH (2-7 percent of original pH value) of peroxide solutions was also observed while moni-

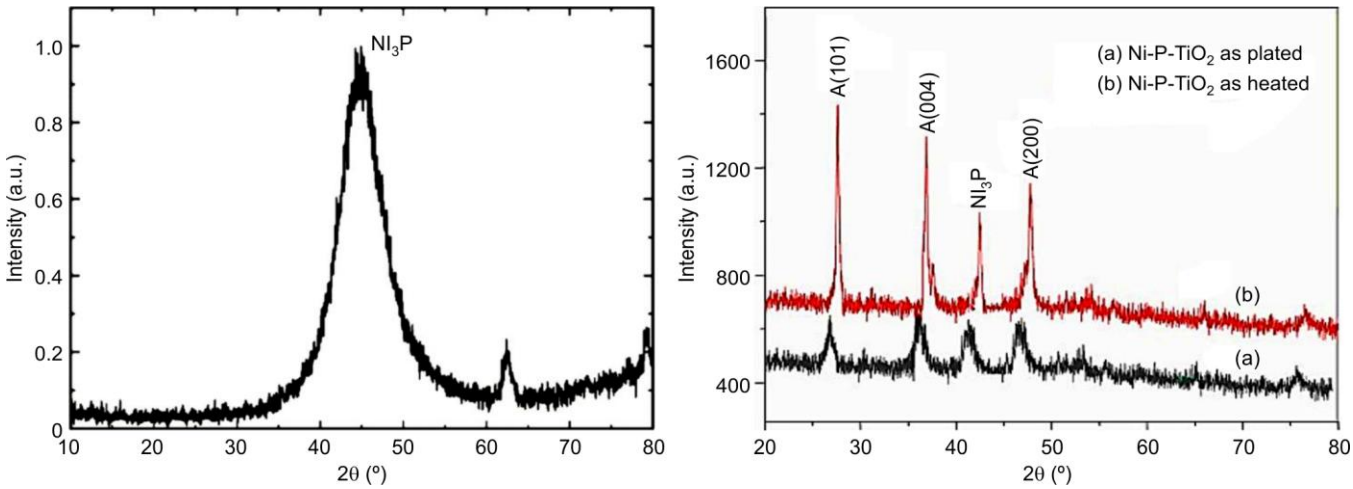

Fig. 3. XRD micrographs of (a) Ni-P (as-plated) and (b) Ni-P-TiO_2 (as-plated and heated) platings

TABLE-4
STOICHIOMETRIC PERCENTAGE (wt.%) OF Ni-P/Ni-P-TiO_2 NANOCOMPOSITE PLATINGS (e ZAF QUANT RESULT ANALYSIS UNCERTAINTY: 5.97%)

Elements	Weight % amount and variation in Ni-P as-plated *vs.* Ni-P heated deposits at 380 ºC	Error %	Weight % amount and variation in Ni-P-TiO_2 as-coated *vs.* Ni-P-TiO_2 heated deposits at 380 ºC	Error %
OK (oxygen)	00.00	00.00	02.81 ± 0.53	04.31
PK (phosphorus)	12.61 ± 0.15	00.72	10.45 ± 0.74	01.87
FeK/L (iron)	04.28 ± 0.56	04.71	03.53 ± 0.25	04.81
NiK/L (nickel)	81.64 ± 0.23	00.64	79.26 ± 0.18	00.52
CK (carbon)	02.08-1.57	06.41	0.85 ± 0.27	03.93
TiK/L (titanium)	00.00	00.00	02.11 ± 0.08	01.14
Total %	100.00%	–	100.00%	–

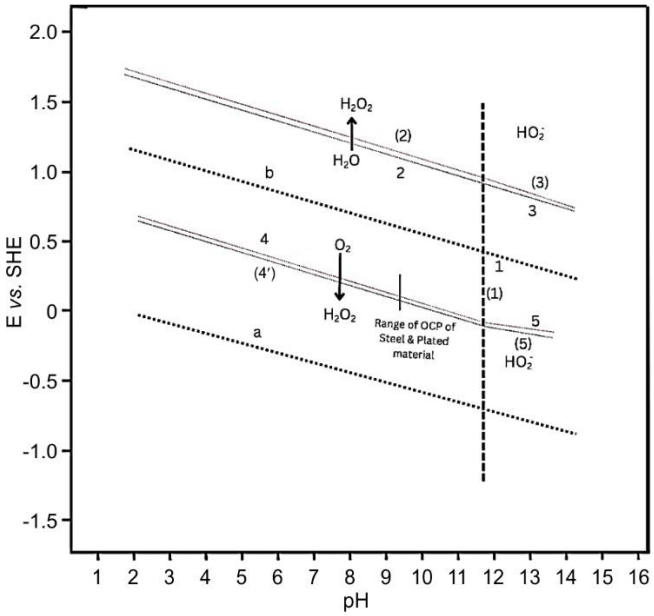

Fig. 4. E-pH diagram for H_2O_2/H_2O system at room temperature

toring pH during both immersion and electrochemical corrosion tests.

The corrosion rate and localized types corrosion attack results for different test steels (MS, SS316L) and Ni-P/Ni-P-TiO_2 plated materials, were evaluated through a long-term immersion and electrochemical corrosion tests into solutions. One main observance in test solutions is that without Cl^- content and low value of H_2O_2 amount (solution 1) solution is the least corrosive and while those of with Cl^- content including higher concentration of H_2O_2 are more corrosive for all the tested materials. The increased corrosivity of peroxide solutions with higher H_2O_2 content may be assigned to H_2O_2/H_2O electrochemical reaction (eqn. 12). The Nernst equation for this eqn. 12 is written as $E_{H_2O_2/H_2O} = 1.78 - 0.059\ pH + 0.0295 \log [H_2O_2]$, and an increase in the concentration of H_2O_2 will shift $E_{H_2O_2/H_2O}$/log I towards higher potential values and thereby increasing an open circuit potential (OCP)/E_{corr} value and consequently corrosion attack on tested materials. The enhanced corrosivity due to increased level of Cl^- may be attributed to the formation of soluble metal chlorides in presence of oxygen, which consequently can decreased the passivation range of steels and Ni-P platings. Through long term immersion corrosion test, the localized and general types corrosion attack on as-plated Ni-P-TiO_2 specimen is observed to be the least and while that on the MS is found the maximum value (Table-5). The PRE (pitting resistance equivalent) and crevice resistance (CRE) index were calculated by formulae as:

$$PRE = \%\ Cr + 3.3\%\ Mo + 30\%\ N \quad (14)$$

$$CRE)\ index = \%\ Cr + 3.7\ \%\ Mo + 30\%\ N \quad (15)$$

For SS316L, PRE was calculated to be 34.814 while that of mild steel (MS) was 0. As these materials (SS316L and MS) are indicating a lower PRE value, therefore it is anticipated from these materials to perform poorly in highly oxidizing solutions against localized corrosion attack [40]. Moreover, for increased peroxide and chloride content solutions, there is found a more rapidly reduction in resistance against localized corrosion for all test coupons. Better resistance of as-plated Ni-P-TiO_2 coupon as compared to other materials may be associated with presence of TiO_2 nanoparticles in the Ni-P matrix, which can create a barrier that restricts the diffusion of corrosive agents such as chloride ions into the plating/substrate surface. The TiO_2 nanoparticles can also act as inert filler by reducing the effective surface area of Ni-P alloy exposed to the corrosive environment and formation of more stable phases as Ni_3P, Ni_3Ti and NiO, which are less susceptible to corrosion and their formations are verified in the XRD results analysis too [5,8,13,17-26]. In electrochemical tests, the MS coupons is tested only through OCP and Tafel curves, as it revealed the highest corrosion rate calculated through long term immersion corrosion test. The

TABLE-5
CORROSION RATE (mpy*) OF TEST COUPONS IN PEROXIDE SOLUTIONS (pH 9.1 ± 0.1)

Alloys	Parameters	Solution 1	Solution 2	Solution 3	Solution 4
MS	Corrosion rate (mpy)	10.26 ± 0.01	12.98 ± 0.01	13.72 ± 0.01	16.21 ± 0.01
	Pitting attack (μm)	17 ± 1	22 ± 1	31 ± 1	52 ± 1
	Crevice attack (μm)	21 ± 1	20 ± 1	34 ± 1	63 ± 1
SS 316L	Corrosion rate (mpy)	0.19 ± 0.01	0.11 ± 0.01	0.32 ± 0.01	0.61 ± 0.01
	Pitting attack (μm)	20 ± 1	29 ± 1	43 ± 1	56 ± 1
	Crevice attack (μm)	18 ± 1	37 ± 1	48 ± 1	51 ± 1
Ni-P (as-plated)	Corrosion rate (mpy)	0.11 ± 0.01	0.17 ± 0.01	0.31 ± 0.01	0.72 ± 0.01
	Pitting attack (μm)	16 ± 1	25 ± 1	40 ± 1	48 ± 1
	Crevice attack (μm)	17 ± 1	29 ± 1	39 ± 1	44 ± 1
Ni-P (heated 380 ºC)	Corrosion rate (mpy)	0.14 ± 0.01	0.19 ± 0.01	0.35 ± 0.01	0.50 ± 0.01
	Pitting attack (μm)	21 ± 1	28 ± 1	43 ± 1	53 ± 1
	Crevice attack (μm)	18 ± 1	34 ± 1	45 ± 1	61 ± 1
Ni-P-TiO_2 (as-plated)	Corrosion rate (mpy)	0.10 ± 0.01	0.12 ± 0.01	0.17 ± 0.01	0.23 ± 0.01
	Pitting attack (μm)	10 ± 1	16 ± 1	21 ± 1	32 ± 1
	Crevice attack (μm)	11 ± 1	18 ± 1	23 ± 1	30 ± 1
Ni-P-TiO_2 (heated 380 ºC)	Corrosion rate (mpy)	0.09 ± 0.01	0.13 ± 0.01	0.18 ± 0.01	0.26 ± 0.01
	Pitting attack (μm)	13 ± 1	20 ± 1	22 ± 1	37 ± 1
	Crevice attack (μm)	15 ± 1	19 ± 1	25 ± 1	33 ± 1

*mpy = mils per year

OCP values for all tested coupons in all solutions are lying into the range of -385.34 to 41.42 mV (-143.34 to 283.42 mV with respect to SHE). The E_{corr} values are found less than OCP values because for OCP measurement, one has to run the experiment for longer duration and so potential rises with built up of some oxide layers on the tested coupons. The OCP/E_{corr} values is also found higher side positive for as-plated Ni-P-TiO_2 coupon in all solutions as compared to other test coupons and generally more positive OCP/E_{corr} values for a coupon in a test solution is an indication of more stable oxide layer formation on that substrate surface. Among all electrochemically obtained cyclic corrosion tested coupons in all solutions, the passivation range (E_c – E_{corr}) for SS316L coupons is found the lower values and while that of the maximum for as-plated Ni-P-TiO_2 coupon. The polarization curves of the as-plated Ni-P-TiO_2 coupon depositions illustrate steady passive character after seeing a vertical passive section and the character of heated curves is not so vertical, which indicate an elevated current at given potential (Fig. 5). The lower performance against corrosive attack into heated Ni-P-TiO_2 coupon as compared to as-plated Ni-P-TiO_2 coupon can be attributed as phase transformations (amorphous to semi-crystalline), different temperature coefficient of expansion of substrate/plate material and growth of larger grains, which can further build weak spots and pathways for corrosive agents to infiltrate these platings [17-26,34,37-42]. Moreover, in the context of corrosion resistance, the Shannon entropy can also be used to quantify the complexity or disorder of a surface. A surface with a higher Shannon entropy value has a more complex and varied texture and this increased complexity can enhance the mechanical interlocking between the plating and the substrate and this stronger interlocking can make it more difficult for corrosive substances to penetrate the plating and reach the underlying material, thus improving corrosion resistance as in as-plated Ni-P-TiO_2 coupon (Shannon entropy value *versus* local value was = 7.344/7.0) (Fig. 6). While, a surface with a lower Shannon entropy is more uniform and less complex and this can result in a weaker mechanical bond between the plating and substrate and potentially making the plating more susceptible to corrosion as in heated Ni-P-TiO_2 coupon (Shannon entropy value versus local value = 6.518/7) [29-31]. Thus, by and large on the basis of E-pH diagram, Shannon entropy values, long term immersion and electrochemical corrosion tests; the tested materials may be graded in terms of their resistance against uniform and localized corrosion in the following manner: Ni-P-TiO_2 as-plated > Ni-P-TiO_2 heated > Ni-P as-plated > Ni-P heated ~SS316L > MS. Better cost/strength ratio of Ni-P-TiO_2 platings can make these materials as more suitable for handling peroxide media with/without Cl^- content.

Conclusion

The SEM/EDAX and XRD investigation reveals that Ni-P/Ni-P-TiO_2 nanocomposite platings are deposited successfully on mild steel substrate. The plating appeared silverish in colour to the naked eye. As-plated Ni-P and Ni-P-TiO_2 coupons exhibited an amorphous structure, while heat-treated Ni-P and Ni-P-TiO_2 coupons revealed a semi-crystalline structure. The corrosivity of tested solutions increases with increase in H_2O_2 and Cl^- ion content. The electrochemical polarization tests, weight loss corrosion test, construction of E-pH diagram of peroxide-water system at room temperature and alongside Shannon entropy values results concluded that alkaline H_2O_2 solutions with/without Cl^- ions are more corrosive against tested steel materials (MS and SS316L) as compared to plated Ni-P/Ni-P-TiO_2 materials. The optimum material for handling tested hydrogen peroxide media is suggested to be as-plated/heated Ni-P-TiO_2 platings in the event of paper mills practices for filtrate recycling.

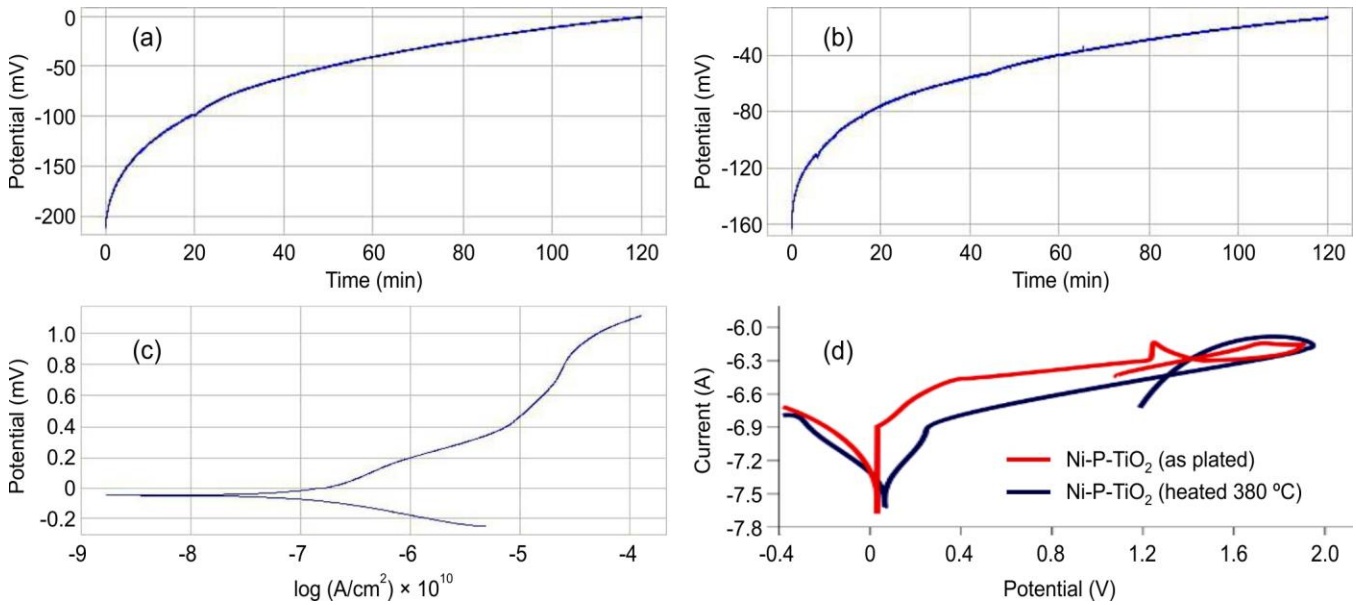

Fig. 5. Electrochemical polarization curve in peroxide solutions of (a) OCP curve of SS316L in solution number 1 (b) OCP curve As-plated Ni-P-TiO_2 plating in solution number 4 (c) potentiodynamic polarization curve of Ni-P (heated) solution number 1 (d) cyclic polarization curve of Ni-P-TiO_2 (as-plated and heated) solution number 4

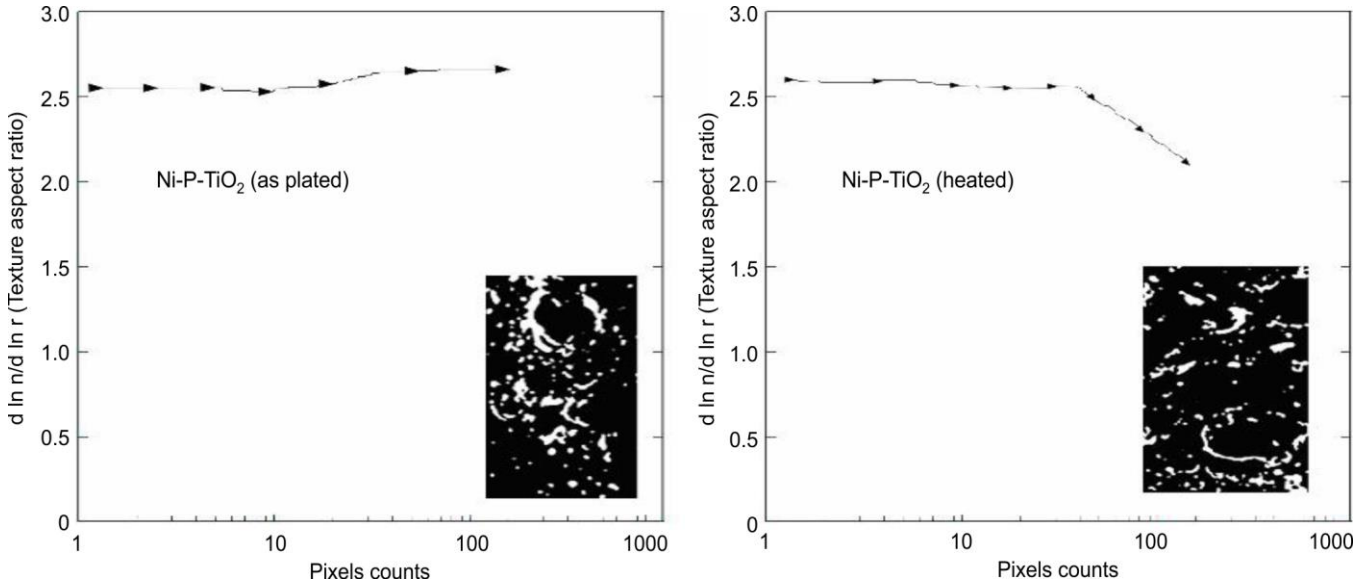

Fig. 6. Shannon entropy curves for as-plated Ni-P-TiO_2 and heated Ni-P-TiO_2 platings

CONFLICT OF INTEREST

The authors declare that there is no conflict of interests regarding the publication of this article.

REFERENCES

1. R. Aslam, M. Mobin, S. Zehra and J. Aslam, *J. Mol. Liq.*, **364**, 119992 (2022); https://doi.org/10.1016/j.molliq.2022.119992
2. B. Fotovvati, N. Namdari and A. Dehghanghadikolaei, *J. Manuf. Mater. Process.*, **3**, 28 (2019); https://doi.org/10.3390/jmmp3010028
3. A. Al-Azzawi and P. Baumli, *Mater. Sci. Eng.*, **40**, 26 (2015).
4. J. Jeevanandam, A. Barhoum, Y.S. Chan, A. Dufresne and M.K. Danquah, *Beilstein J. Nanotechnol.*, **9**, 1050 (2018); https://doi.org/10.3762/bjnano.9.98
5. J. Sudagar, J. Lian and W. Sha, *J. Alloys Compd.*, **571**, 183 (2013); https://doi.org/10.1016/j.jallcom.2013.03.107
6. D. Seifzadeh and Z. Rajabalizadeh, *Surf. Coat. Technol.*, **218**, 119 (2013); https://doi.org/10.1016/j.surfcoat.2012.12.039
7. Y. De Hazan, F. Knies, D. Burnat, T. Graule, Y. Yamada-Pittini, C. Aneziris and M. Kraak, *J. Colloid Interface Sci.*, **365**, 163 (2012); https://doi.org/10.1016/j.jcis.2011.09.032
8. M. Ram, S. Sharma, A. Ansari and A.K. Sharma, *AIP Conf. Proc.* **2335**, 080010 (2021); https://doi.org/10.1063/5.0043715
9. H. Luo, M. Leitch, H. Zeng and J.-L. Luo, *Mater. Today Phys.*, **4**, 36 (2018); https://doi.org/10.1016/j.mtphys.2018.03.001
10. D.R. Dhakal, G. Gyawali, Y.K. Kshetri, J.-H. Choi and S.W. Lee, *Surf. Coat. Technol.*, **381**, 125135 (2020); https://doi.org/10.1016/j.surfcoat.2019.125135
11. A. Mukhopadhyay, T.K. Barman and P. Sahoo, *Tribol. Trans.*, **61**, 41 (2018); https://doi.org/10.1080/10402004.2016.1271929
12. D.H. Xia, C. Deng, D. Macdonald, S. Jamali, D. Mills, J.L. Luo, M.G. Strebl, M. Amiri, W. Jin, S. Song and W. Hu, *J. Mater. Sci. Technol.*, **112**, 151 (2022); https://doi.org/10.1016/j.jmst.2021.11.004
13. U.D. Bagale, S.H. Sonawane, B.A. Bhanvase, R.D. Kulkarni and P.R. Gogate, *Green Process Synth.*, **7**, 147 (2018); https://doi.org/10.1515/gps-2016-0160
14. T. Chen, B. Wang, Z. Qi, Z. Guo, Y. Tian and F. Meng, *ACS Appl. Nano Mater.*, **5**, 9780 (2022); https://doi.org/10.1021/acsanm.2c01993
15. Y. Li, N. Kawashima, J. Li, A.P. Chandra and A.R. Gerson, *Adv. Colloid Interface Sci.*, **1**, 197-198 (2013); https://doi.org/10.1016/j.cis.2013.03.004
16. H. Nazari, G.B. Darband and R. Arefinia, *J. Mater. Sci.*, **58**, 4292 (2023); https://doi.org/10.1007/s10853-023-08281-1
17. M.A. Shoeib, M.M. Kamel, S.M. Rashwan and O.M. Hafez, *Surf. Interface Anal.*, **47**, 672 (2015); https://doi.org/10.1002/sia.5764
18. J. Novakovic, P. Vassiliou, K.L. Samara and T. Argyropoulos, *Surf. Coat. Tech.*, **201**, 895 (2006); https://doi.org/10.1016/j.surfcoat.2006.01.005
19. H. Chakhtouna, H. Benzeid, N. Zari, A. Qaiss and R. Bouhfid, *Environ. Sci. Pollut. Res. Int.*, **28**, 44638 (2021); https://doi.org/10.1007/s11356-021-14996-y
20. Y. Nosaka, *Catalysts*, **12**, 1557 (2022); https://doi.org/10.3390/catal12121557
21. M.T. Noman, M.A. Ashraf and A. Ali, *Environ. Sci. Pollut. Res. Int.*, **26**, 3262 (2019); https://doi.org/10.1007/s11356-018-3884-z
22. Q. Zhao, C. Liu, X. Su, S. Zhang, W. Song, S. Wang, G. Ning, J. Ye, Y. Lin and W. Gong, *Appl. Surf. Sci.*, **274**, 101 (2013); https://doi.org/10.1016/j.apsusc.2013.02.112
23. W. Chen, W. Gao and Y. He, *Surf. Coat. Technol.*, **204**, 2493 (2010); https://doi.org/10.1016/j.surfcoat.2010.01.032
24. M.S. Hasan, F. Zemajtis, M. Nosonovsky and K. Sobolev, *J. Tribol.*, **144**, 081402 (2022); https://doi.org/10.1115/1.4053777
25. S. Akhtar, K. Shahzad, S. Mushtaq, I. Ali, M.H. Rafe and S.M. Fazal Ul-Karim, *Mater. Res. Express*, **6**, 105409 (2019); https://doi.org/10.1088/2053-1591/ab3b27
26. A. Bachvarova-Nedelcheva, R. Iordanova, A. Naydenov, A. Stoyanova, N. Georgieva, V. Nemska and T. Foteva, *Catalysts*, **13**, 257 (2023); https://doi.org/10.3390/catal13020257
27. P.M. Kallel, Z. Anther, M. Masseoud, S. Vesco, M. Barletta and k. Elleuch, *Ceramics Int.*, **47**, 10 (202 1); https://doi.org/10.1016/j.ceramint.2021.02.023

28. G. John, M.E. Sahayaraj, J.T.W. Jappes and S.J. Leon, *Period. Mineral.*, **92**, 67 (2023); https://doi.org/10.37896/pd92.2/9224
29. I. Vranken, J. Baudry, M. Aubinet, M. Visser and J. Bogaert, *Landsc. Ecol.*, **30**, 51 (2015); https://doi.org/10.1007/s10980-014-0105-0
30. X. Zhang, X. Dai, L. Gao, D. Xu, H. Wan, Y. Wang and L. Yan, *Chem. Soc. Rev.*, **52**, 6806 (2023); https://doi.org/10.1039/D3CS00347G
31. J.L. Braun, C.M. Rost, M. Lim, A. Giri, D.H. Olson, G.N. Kotsonis, G. Stan, D.W. Brenner, J.-P. Maria and P.E. Hopkins, *Adv. Mater.*, **30**, 1805004 (2018); https://doi.org/10.1002/adma.201805004
32. A. Sharma, Ph.D. Thesis, Corrosion Investigations in Pulping and Bleaching Media, Indian Institute of Technology Roorkee, Roorkee, India (2006).
33. J. Kisel, Ph.D. Thesis, Study of Tin(II)/Tin(IV)/Anhydrous Hydrochloric Acid based Sensitizers for Electroless Deposition, University of Windsor, Canada, National Library of Canada (1989).
34. B.D. Cullity, Elements of X-Rays Diffraction., Addison-Wesley Publishing Co. Inc., Reading Mass, USA (1956).
35. Powder Diffraction File, Joint Committee on Powder Diffraction Standards (JCPDS-File) (1978).
36. S. Sharma and A. Kumar, *J. Mol. Liq.*, **322**, 114862 (2021); https://doi.org/10.1016/j.molliq.2020.114862
37. A.I. Vogel, Quantitative Inorganic Analysis, 296, London, Longman, Green & Co. (1964).
38. ASTM G1-05, Standard Practice for Preparing, Cleaning and Evaluating Corrosion Test Specimens, 3(2) (2025).
39. M. Pourbaix, Atlas of Electrochemical Equilibria in Aqueous Solutions, Houston, NACE, p. 256 (1974).
40. ASTM G78, Standard Guide for Crevice Corrosion Testing of Iron Base and Nickel Base Stainless alloys in Sea water and other chloride containing aqueous Environments., 3(2) (1991).
41. S. Raji, A. Popoola and O. Akanji, *J. Mol. Struct.*, **1312**, 138414 (2024); https://doi.org/10.1016/j.molstruc.2024.138414
42. Y. Fujimori, M. Shimizu, T. Kurashina, and S. Arai, *Mater. Lett.*, **350**, 134869 (2023); https://doi.org/10.1016/j.matlet.2023.134869